Supplementary Information

Customized MFM probes based on magnetic nanorods

Miriam Jaafar*[a,b], Javier Pablo-Navarro[c], Eider Berganza[b,d], Pablo Ares[a], César Magén[c,e,f], Aurélien Masseboeuf[g], Christophe Gatel[g], Etienne Snoeck[g], Julio Gómez-Herrero[a], José María de Teresa[c,e,f], Agustina Asenjo[b]

[a]Departamento de Física de la Materia Condensada and Condensed Matter Physics Center (IFIMAC), Universidad Autónoma de Madrid, 28049 Madrid, Spain.

[b]Instituto de Ciencia de Materiales de Madrid, CSIC, 28049 Madrid, Spain.

[c]Laboratorio de Microscopías Avanzadas - Instituto de Nanociencia de Aragón, Universidad de Zaragoza, 50018 Zaragoza, Spain.

[d]Institute of Nanotechnology, KIT Campus North, 76344 Eggenstein-Leopoldshafen, Germany.

[e]Instituto de Ciencia de Materiales de Aragón, Universidad de Zaragoza-CSIC, 50009 Zaragoza, Spain.

[f]Departamento de Física de la Materia Condensada, Universidad de Zaragoza, 50009 Zaragoza, Spain.

[g]CEMES, CNRS, 29 rue Jeanne Marvig, F-31055 Toulouse, France.

1- DETERMINATION OF THE SWITCHING FIELD OF THE MFM PROBES

In order to determine the switching field of the magnetic force microscopy probes, a reference sample with very high coercive field has been employed, in this case, a hard drive disk. When an area with enough contrast is found, the scan is stopped in one of the lines (for more details see ref. 1 at the end of the SI). The chosen line is continuously scanned, while a magnetic field perpendicular to the sample plane is applied, in the opposite direction to the magnetization of the tip. One can therefore see an inversion in the magnetic contrast at the coercive field of the magnetic probe. As we can see in Figure S1, it is not possible to see the contrast inversion for the case of the Fe-based nanorod but a hysteresis loop can be measured for the Co-based nanorod. In this case, the switching field is higher than the one detected for a *Budget Sensors MagneticMulti75-G* commercial MFM probe. However, for different diameters of Co-based nanorods we observed that the reversal process is sometimes different because of the existence of closure domains for the thicker nanorods.

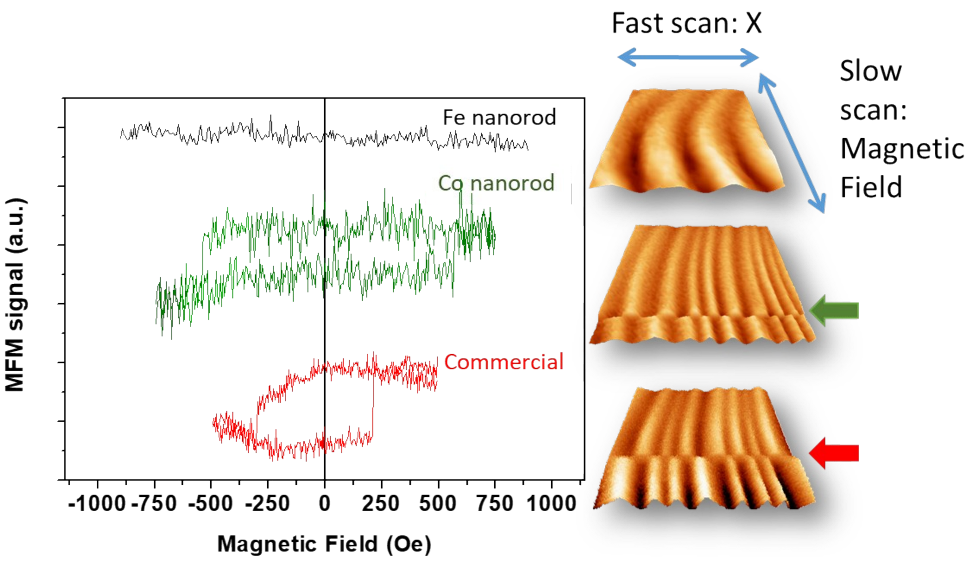

Figure S1. Local hysteresis loops measured by advanced MFM mode.

2- IMPROVING LATERAL RESOLUTION

When it comes to measuring small objects such as the nanoparticles presented in Figure S2, the advantage of using nanorods grown by FEBID is twofold. On the one hand, as shown in the graph from Fig. S2a, with a sharp enough nanorod the lateral resolution can be significantly improved both in the topographic and in the magnetic image (Fig. S2d). On the other hand, the nanorod can be customized in a way that its stray field is low enough to hamper it from causing major modifications in the tip magnetic configuration of very soft samples (Fig. S2e and f). In the graph presented in Fig. S2g the magnetic contrast is plotted as a function of the tip-sample distance when a magnetic dipole is detected. In such situation the two-dipole model, also called the point-probe model, can be used to extract quantitative magnetic information from the MFM data.

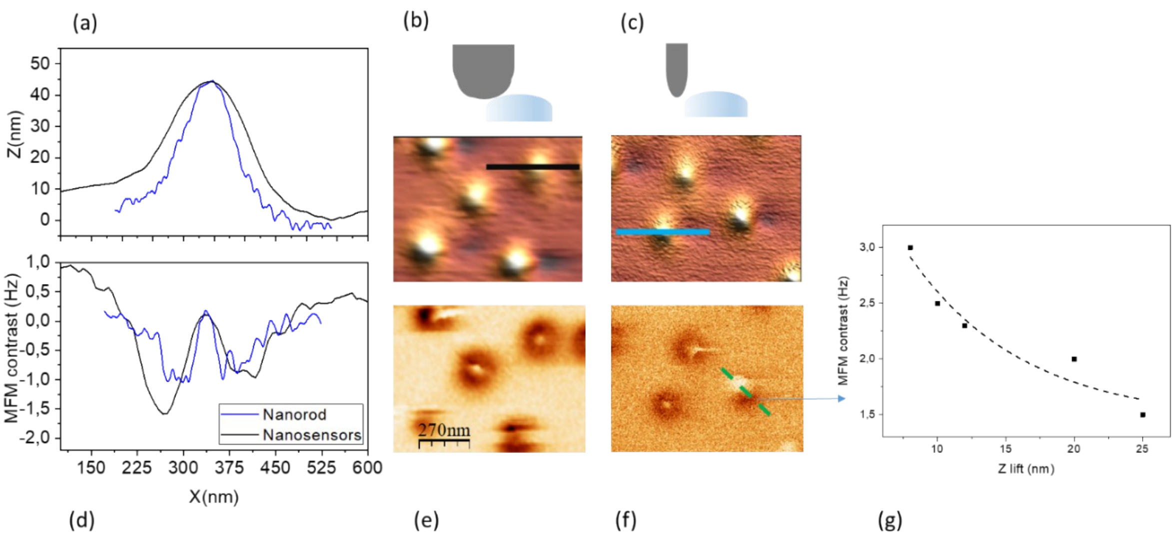

Figure S2. Topographic (a,b,c) and magnetic images and its corresponding profiles (d,e,f) of the same sample obtained with two types of tips: *NanoSensors PPP-MFM* commercial magnetic probe and a Fe-based Nanorod with a sharp tip end of 7 nm. The sample consists of Py magnetic nanoparticles with a diameter of 50 nm in average. (g) MFM contrast across the Py nanodot marked in green in S2(f) for different Z lift distances. The dash line in the graph is a guide for the eye.

3- TIP STRAY FIELD

Regarding the stray field of the tip, it is possible to control it by tuning the shape and composition of the nanorods. Five different nanorods have been analyzed by Electron Holography. The stray fields calculated from those measurements correspond to a broad distribution of fields at the apex of the nanorod, ranging from 80 mT to 260 mT (orange dots).

However, the stray field at the typical MFM distance around 50 nm (blue dots) is quite similar in all cases and it mainly depends on the section of the nanorod which guarantees the reproducibility of the process. As shown in the STEM images of Fig. S9 corresponding to the nanorods 1, 3 and 4 (ordered by section), although the diameter is rather similar, the particular shape of the apex of the nanorod, determined by the growth properties, controls the stray field close to the tip.

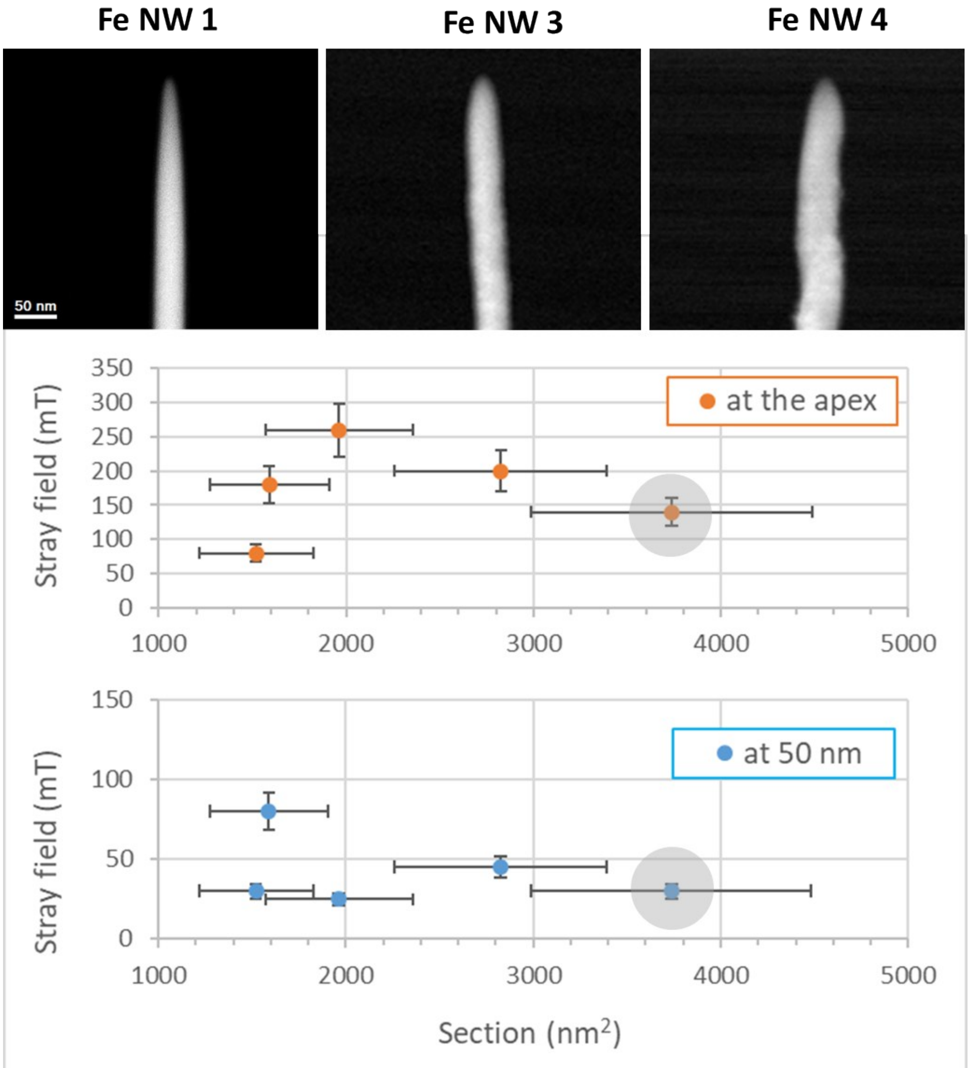

Figure S3. Stray field values calculated from the EH measurements of different Fe-based nanorods with different sections and apex shapes. The values marked in grey correspond to a Co-based nanorod.

4- LOWER VAN DER WAALS PROBE-SAMPLE INTERACTION

In Figure S4a we performed spectroscopic measurements where the dependence of the frequency shift (magnetic signal) with the distance for two kinds of MFM probes (a commercial one with pyramidal geometry and a nanorod-tip) is shown. The sample used is the FePd multilayer with perpendicular magnetic anisotropy. As demonstrated in the graph from Figure S4a, the nanorod allows approaching closer to the surface to obtain the magnetic image from the sample. In the two-pass mode, where the second scan is performed at a typical retrace distance of 20 nm, being able to scan closer entails some benefits, such as improving the lateral resolution of the measurement.

In Figure S4b we compare approaching Force vs. Distance curves for a commercial *Budget Sensors MagneticMulti75-G* probe (typical tip radius < 60 nm according to the manufacturer) and a Co-based nanorod tip with a tip radius of 30 nm (from SEM characterization). As can be seen, the jump-to-contact peaks present significantly different values, with the one from the nanorod tip (around -7.5 nN) being approximately half that of the commercial tip (-15 nN). Since the magnitude of these peaks is related to the attractive forces (usually van der Waals and capillary forces in air), these curves show the reduction of these attractive forces when using nanorod tips.

(a)

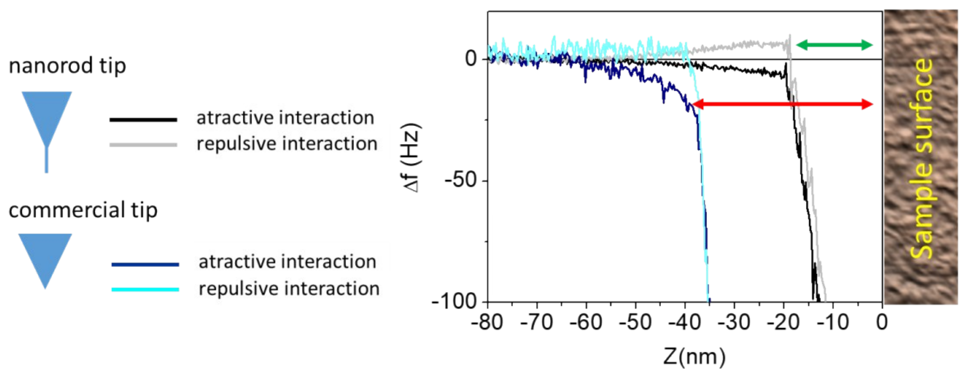

(b)

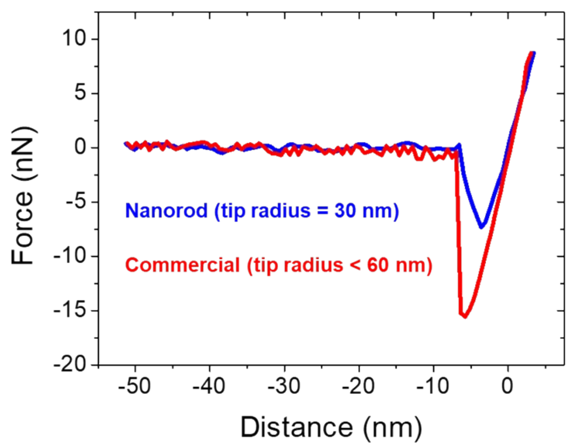

Figure S4. (a) Spectroscopic measurements where the frequency shift versus the tip sample distance is plotted for two kinds of tips: Fe-based nanorod and commercial *Budget Sensors MagneticMulti75-G* MFM probe. (b) Approaching Force vs. Distance curves in air for a commercial *Budget Sensors MagneticMulti75-G* tip (red) and a Co-based nanorod tip (blue). The magnitude of the jump-to-contact point in the case of the nanorod tip is much lower than in the commercial probe, which shows a reduction in the attractive forces (mainly vdW and capillary).

5- IN-PLANE vs. OUT-OF-PLANE SIGNAL

In this work we find that the stray field of the tips can be controlled through the geometry of the nanorods. Fe- and Co-based nanorod tips grown onto similar cantilevers but with different sections have been characterized with two reference samples: (a) FePd thin film with perpendicular anisotropy and (b) a hard disk with In-Plane (IP) magnetization (b). For each nanorod tip, we have obtained MFM images by using the IP and Out-Of-Plane (OOP) reference samples. The average MFM signals (frequency shift) for each tip versus the section of the nanorod is plotted. First, we observe that the higher the IP signal, the lower the OOP contrast and vice versa. Moreover, for the Fe composition, as the nanorod section increases, the OOP contrast decreases and the IP increases. Similar behaviour is observed for the Co-based nanorods, except for the thicker nanorods that present different behaviour probably due to the existence of a closure domain at the end.

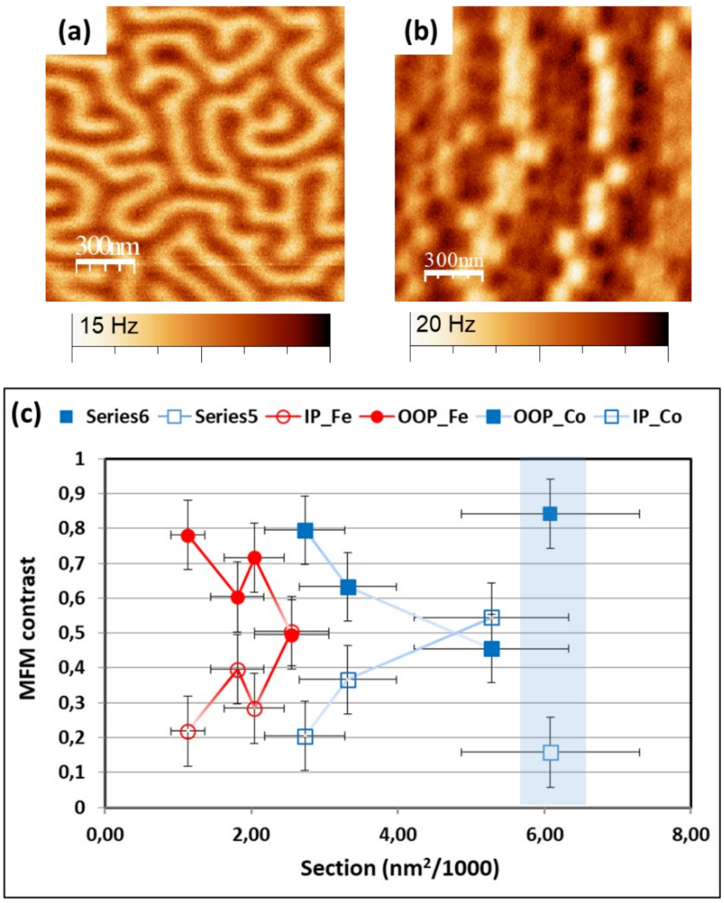

Figure S5. (a) MFM image of a FePd thin film and (b) MFM image of a hard disk reference sample measured with an Fe-based nanorod. (c) Average MFM signal (normalized contrast *versus* section of the nanorods. The data in the shadow region correspond to the thicker Co nanorods that present different behaviour.

6- SIGNAL TO NOISE RATIO IMPROVEMENT

It is well-known that in atomic force microscopy selecting a cantilever with a smaller spring constant theoretically enhances the sensitivity. Nevertheless, this also reduces its resonance frequency, which results in a larger noise level, worsening the frequency shift detection which is the crucial parameter for the MFM measurements. A standard study of fundamental MFM noise shows that further improvement on the performance could be gained through the use of specially designed cantilevers. However, typical MFM probes available at present in the market are mounted on cantilevers with resonance frequencies and spring constants of about 70 kHz and 0.7–3 N/m. The frequency shift of a vibrating cantilever in the presence of a force gradient is proportional to the factor ω_0/k. In Figure S6 we demonstrate that FEBID probes can be used to enhance the signal to noise ratio in MFM measurements. Similar Fe–based magnetic FEBID tips (length ~1.7 μm and 50 nm in diameter) have been grown on non-magnetic cantilevers with very different geometrical parameters (see Figure S6 a-b): *Budget Sensors* non-magnetic levers with resonance frequency and spring constant of 65 kHz and 2.5 N/m, named as *standard* in the following analysis, and *Olympus BL-AC40TS-C2* with resonance frequency and spring constant of 88 kHz and 0.07 N/m, respectively, named as *soft*. The Sader Method has been used to calculate the value of the spring constants (ref. 2). The performance of the nanorods has been compared using a high-density hard disk as a reference sample.

Figure S6 c-d shows the magnetic images obtained with those probes and their corresponding profiles (Fig. S6 e-f). On the one hand, for the *standard* cantilever, we obtain a factor in air-ambient conditions $(\omega_0/k)_{standard}$ ~ 1.7 x10^5 rad·N/s·m. On the other hand, for the *soft* cantilever, the same factor has a value of 7.8 x 10^6 rad·N/s·m. The ratio between these two factors leads to a ~ 47-fold improvement in the frequency shift sensitivity. But the use of lower force constant cantilevers will result in an increase in the fundamental noise level of the measurement, worsening the frequency shift sensitivity. This noise increase is proportional to $\sqrt{1/kQ}$ (see ref. 3), with *k* the cantilever stiffness and *Q* the quality factor of the resonance. For the *standard* cantilever this factor is ~ 0.04 $(N^{-1}\,m)^{1/2}$ whereas for the *soft* cantilever it achieves a value of ~ 0.6 $(N^{-1}\,m)^{1/2}$. The ratio between these two factors leads to a ~ 15-fold worsening in the frequency shift.

By using these *soft* cantilevers, on one side the frequency shift sensitivity would improve a factor of ~ 47 and in the other side it would worsen a factor of ~ 15, resulting in a final improvement of a factor of 47/15, roughly ~ 3. Figure S6 c-f shows a remarkable increase in the magnetic signal for the soft cantilevers (note the different values for the colour tables).

The advantages of the FEBID tips in this study are several: first, for these particular soft cantilevers the companies advise the costumer that its use is not recommended at ambient conditions. We demonstrate that after the growth of the nanorods, this kind of levers can be used both in air and in liquid conditions. In fact, the measurements in liquid have even a better improvement in the signal to noise ratio (~4). Secondly, the functionalization of these soft levers by sputtering is not as easy as for the case of standard cantilevers while the growth of the nanorods is completely reproducible. And finally, as we demonstrate in the main text, we can achieve tips with final radius less than 10 nm, so it is possible to enhance the sensitivity by using soft cantilevers keeping a very good lateral resolution in the MFM image.

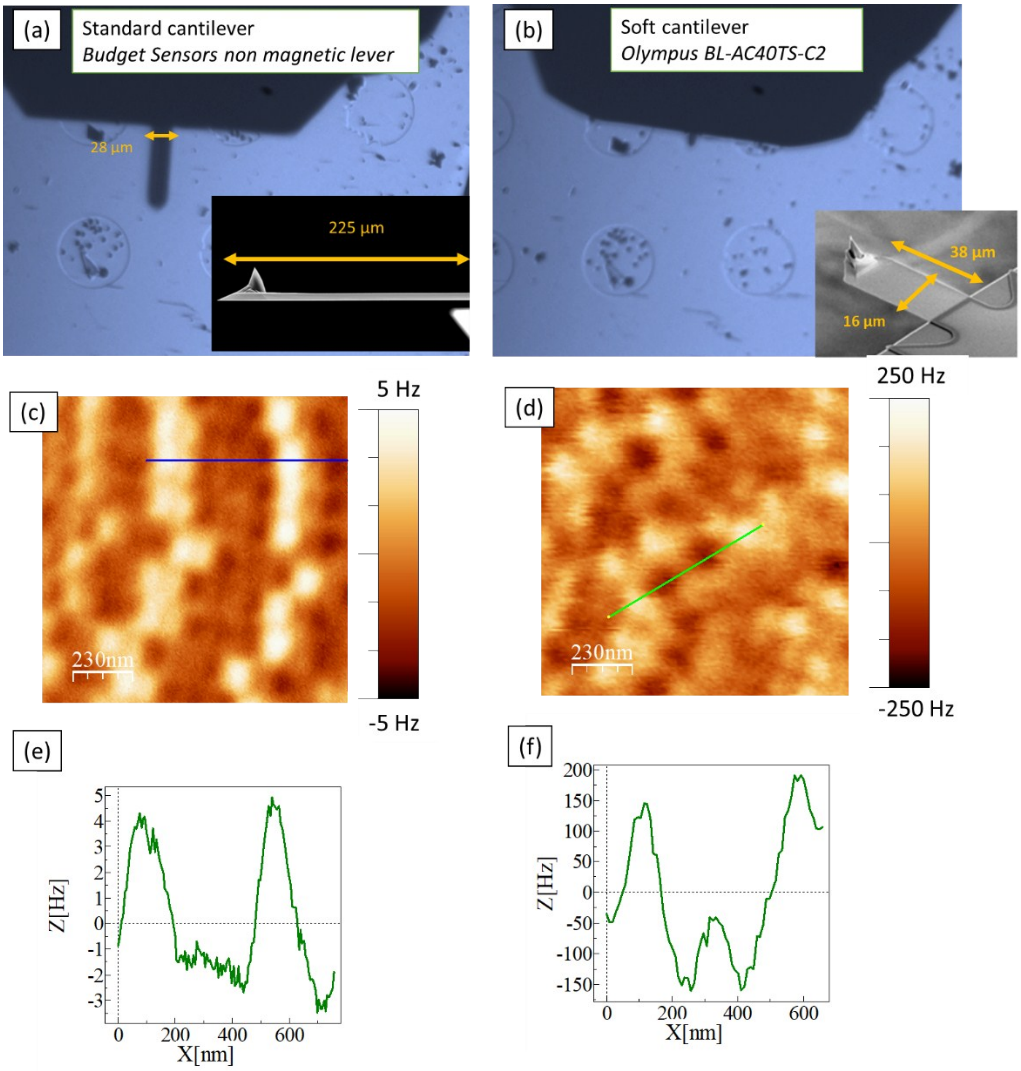

Figure S6. (a) and (b) are optical images of a standard cantilever and a soft *Biolever*. The differences between the two cantilevers are clearly visible (see insets for more details). (c) and (d) are magnetic images of a hard disk reference sample acquired with two similar based Fe-FEBID nanorods (L~1.7 µm and 50 nm in diameter) grown onto the two levers shown in (a)-(b). The images are taken at ambient conditions. (e) and (f) are the corresponding profiles where the improvement of the signal to noise ratio is shown.

It is worth mentioning that the evaluation of the normalized MFM contrast in Figure 3 (main text) is calculated following this procedure: (a) two Gaussian curves are fitted to the experimental MFM signal distribution, the MFM contrast for each image is stablished as the increment between the centres of the Gaussian curves, (b) the magnetic contrast is normalized taking into account equation (1) where f_0 is the free frequency and k is the constant force of each probe calculated by the Sader method by using the experimental values of f_0 and Q factor, (c) the magnetic moment of the two kinds of probes (Ms tip =1190 emu/cm^3 for Fe-based tips and 600 emu/cm^3 for the CoCr one) has been also considered to separate the geometric effect, (d) the errors in the section are determined by the resolution of the SEM images of the nanorod tips, except for the commercial probe, determined from a statistic of the lateral resolution of several topography images. Moreover, the error in the MFM contrast is evaluated from the noise of the experimental MFM images (higher than the error of the fitting).

$$\Delta\emptyset \approx \frac{f_0 \partial F}{2k\partial z} \qquad (1)$$

We assume that $\frac{\partial F}{\partial z} \sim M_{s\,tip}$

7- CONTROL OF THE MAGNETIC PROPERTIES OF THE NANORODS: DEGRADATION OF THE MAGNETIC PROPERTIES. CORE-SHELL PROBES

The idea of growing a core-shell structure that can protect the magnetic core of the nanorod could be useful for some experiments. On the one hand, it minimizes the surface oxidation of the core to a non-ferromagnetic material. On the other hand, the combination of more than one material with different physical properties in the MFM probe allows the addition of different functionalities to the experiment.

MFM images of a reference sample obtained with two types of Fe-FEBID probes (grown onto 3 N/m non-magnetic *Budget Sensors ElectriMulti75-G* cantilevers) are presented in Figure S7. The MFM image in Figure S7a has been obtained with one Fe-based nanorod similar to the one presented in Figure 3c of the main text. The magnetic image in Fig. S7b has been acquired with a core-shell structure. The geometrical properties of the magnetic cores are very similar in both cases.

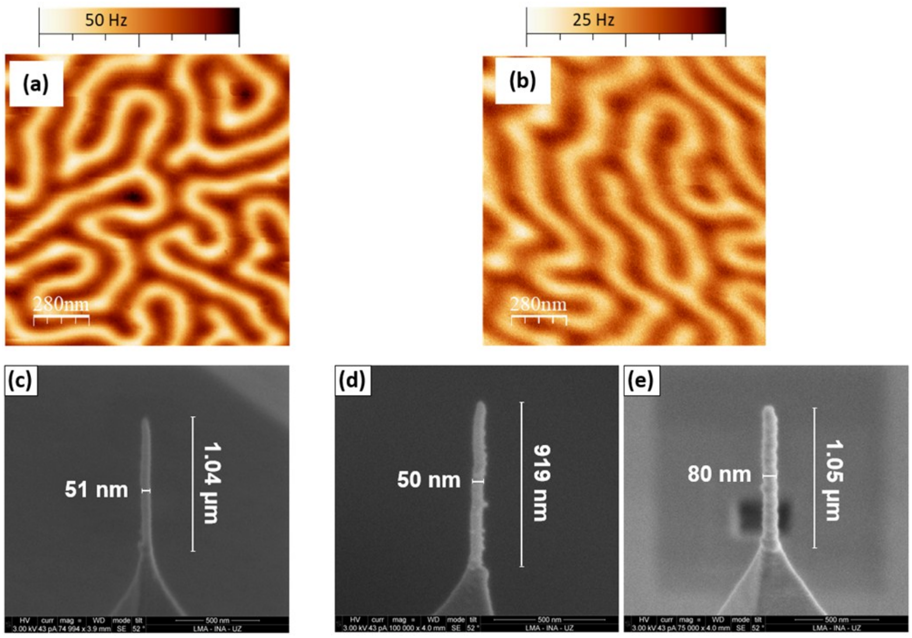

Figure S7. MFM images of a FePd multilayer with perpendicular magnetic anisotropy obtained with an Fe-based nanorod (a) and a core-shell PtC-Fe nanorod (b). SEM images of a (c) Fe nanorod, and (d)-(e) core-shell Fe-@PtC nanorod (d) before and (e) after the PtC coating.

In addition, the growth of this kind of core-shell nanorods is also possible on cantilevers with low force constants (Biolever ones) and can be useful for measurements under physiological conditions. As we can see in Figure S8 this structure maintains a good SNR.

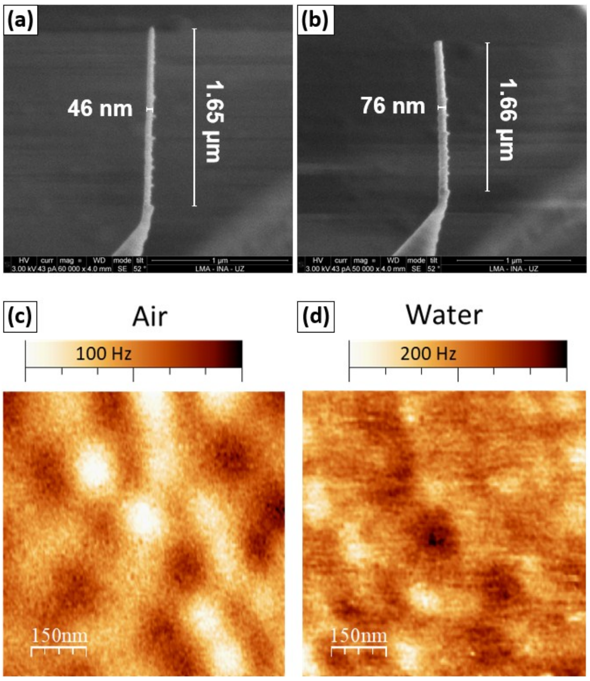

Figure S8. Core-shell Fe-@PtC nanorod grown onto non-magnetic *Biolever* mini (a) before and (b) after the PtC coating. MFM images acquired in (c) air and (d) water of a hard-disk reference sample.

Nevertheless, the performance of Fe-based nanorods without the protective layer has been checked after measurements in water. In Figure S9 we can observe that the quality of the magnetic signal after the immersion of the nanorod has not been affected.

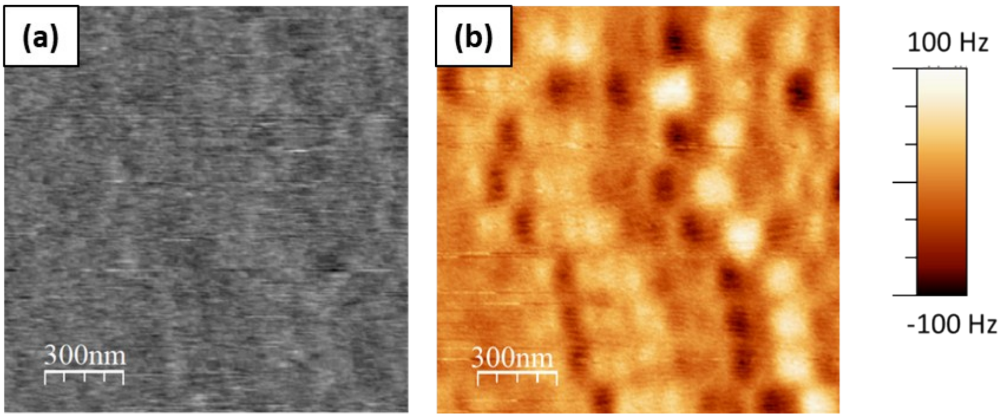

Figure S9. Topography (a) and MFM (b) images of a hard disk reference sample acquired with an Fe-based nanorod onto a Biolever probe. Air measurements after drying probe and sample.

REFERENCES

[1] Jaafar, M.; Serrano-Ramón, L.; Iglesias-Freire, O.; Fernández-Pacheco, A.; Ibarra, M. R.; de Teresa, J. M.; Asenjo, A. Hysteresis Loops of Individual Co Nanostripes Measured by Magnetic Force Microscopy. Nanoscale Res. Lett. 2011, 6, 407.
[2] Sader, J. E.; Chon, J. W. M.; Mulvaney, P. Calibration of rectangular atomic force microscope cantilevers. Rev. Sci. Instrum. 1999, 70, 3967-3969.
[3] Garcia, R.; Perez, R. Dynamic atomic force microscopy methods. Surf. Sci. Rep. 2002, 47, 197-301.